Trace metal analysis of sediment cores using a novel X-ray Fluorescence core scanning method

Rick Hennekam[a,*], Tim Sweere[b], Rik Tjallingii[c], Gert J. de Lange[b], Gert-Jan Reichart[a, b]

* Corresponding author. E-mail address: rick.hennekam@gmail.com

[a] NIOZ Royal Netherlands Institute for Sea Research, Department of Ocean Systems, and Utrecht University, P.O. Box 59, 1790 AB Den Burg, Texel, The Netherlands

[b] Department of Earth Sciences, Faculty of Geosciences, Utrecht University, P.O. Box 80.121, 3508 TA Utrecht, The Netherlands

[c] GFZ German Research Centre for Geosciences, Section 5.2 – Climate Dynamics and Landscape Evolution, Potsdam, Germany

Abstract

The trace-metal composition of sediments provides important information on (past) environmental conditions, such as bottom water oxygenation, marine productivity, sediment provenance, and pollution. Whereas major and minor elements are often routinely analyzed using X-Ray Fluorescence (XRF) core scanning, analysis of trace metals with the same method is not yet established as a routine procedure. Here, we used a recently developed state-of-the-art XRF detector with a core scanner (Avaatech) to examine the optimal settings for analyzing a suite of trace metals (V, Cr, Ni, Cu, Zn, Mo, and U). Settings were optimized for fast analyses of sediment cores by extensive testing of primary energy settings, filters, and exposure times on two eastern Mediterranean Sea sapropel layers that archive episodes of past sea-floor anoxia. We reveal the following most advantageous (i.e., optimized for analytical accuracy and time efficiency) settings: (1) V, Cr, Ni at 20kV with aluminum primary beam filter, (2) Cu, Zn, and U at 30kV with 'thick' (125 μm) palladium primary beam filter, and (3) Mo at 50kV with copper primary beam filter. For these trace elements, generally, ≥30 seconds of measurement are required for obtaining reliable data. Synthetic mixtures show that matrix effects, which are inherent to XRF analyses, are of particular importance for V. A correction for these matrix effects on V (e.g., using Compton scattering) may be necessary for samples with a large variability in carbonate content. XRF core-scanning measurements on synthetically, laminated sediments show that trace metals with contrasting atomic weights and related XRF penetration depths (V and Mo) can be determined at sub-mm resolution. We show that intensity results from the new XRF detector can be converted into concentrations using multivariate log-ratio calibration, allowing a fast quantitative prediction of sedimentary trace metal content using XRF core scanning.

Keywords

Trace metals, XRF core scanning, high-resolution geochemistry, paleoclimate, paleoenvironment

1. Introduction

The concentrations of trace metals in sedimentary archives provide important constraints on past environmental conditions. For instance, sedimentary concentrations of vanadium (V), chromium (Cr), molybdenum (Mo), and uranium (U), record past oxygenation of the oceans, because their solubility is related to the redox state (Algeo and Lyons, 2006; Brumsack, 2006; Tribovillard et al., 2006, 2012; Algeo and Tribovillard, 2009; Algeo and Rowe, 2012; Sweere et al., 2016). The sedimentary distribution for trace metals such as nickel (Ni), copper (Cu), and zinc (Zn) can also be associated to organic-matter sinking rate in the water column, potentially delivering information on export productivity (Bruland, 1980; Brumsack, 2006; Tribovillard et al., 2006). Moreover, trace metals are useful for sediment provenance discrimination (Garver et al., 1996; Yang et al., 2003), and detection of sediment pollution (Ruiz, 2001). Conventional analyses of trace metals in sediments involve total destruction with strong acids followed by, e.g., Inductively Coupled Plasma-Mass Spectrometry (ICP-MS) analyses, or glass-bead preparation followed by off-line X-Ray Fluorescence (XRF) analyses. Although these methods are well established, they are also time consuming and costly. To address this issue, the use of XRF core scanning to determine sedimentary trace metal profiles is explored here.

XRF core scanning (XCS) is renowned for fast and high-resolution (up to <mm) sediment measurements, with relatively little cost (Croudace and Rothwell, 2015). Studies using XCS usually focus on major and minor elements, but trace metals such as Mo have also been analyzed (Wirth et al., 2013; Gibson and Peterson, 2014). Nonetheless, especially combinations of multiple trace metals provide powerful paleo-environmental proxies, such as the covariation of V, Mo, and U (Algeo and Tribovillard, 2009; Tribovillard et al., 2012), and, currently, these trace metals are not routinely measured by XCS. State-of-the-art digital silicon drift detectors, with increased detection speed and improved spectral resolution (~125 eV at Mn-Kα) have recently become available and are potentially capable of in-situ trace-metal analyses on sediment surfaces using XCS. Here, we investigate the suitability of these new XRF detectors and describe the optimal methodology for trace metal analyses.

We present a systematic study aimed at establishing trace metal analyses using XCS, for which we use 4 consecutive steps. 1. The optimal instrumental settings for trace element analyses are investigated. Specifically, we extensively test different combinations of X-Ray tube-energy settings, primary-beam filters, and analytical dwell times for 22 samples with known compositions. 2. Optimized XCS settings for trace-metal analyses are applied to long sediment core records with known trace-metal distributions from the eastern Mediterranean Sea. The sedimentary sequence used contains two past intervals of basin-wide anoxia and enhanced organic-matter deposition (i.e., sapropels, see Rohling et al., 2015). Analyses are performed on wet core material and on dry powdered samples, to study the effects of interstitial water that can alter XCS measurements (Tjallingii et al., 2007; Hennekam and De Lange, 2012). The XCS data are converted to

concentrations using a multivariate log-ratio calibration approach (Weltje et al., 2015) to evaluate XCS as a tool to perform fast quantitative geochemical predictions. 3. XCS measurements are performed on artificially produced laminations with set variable V and Mo concentrations, to deduce the potential effects of sub-mm-scale XRF scanning on elements of contrasting atomic weights. 4. Sediment samples of three common matrices (i.e., quartz, clay, and calcite) were spiked with known amounts of trace metals and used to assess potential matrix effects for V and Mo. The focus is on V, as its K-line energies are in the middle of a wide range of major elements (K, Ca, Ti, Mn, Fe), which generally cause the strongest matrix effects (Croudace and Gilligan, 1990).

Optimal XCS settings for trace metal analyses established in this study are also considered for a wider range of detectors. For this, we performed tests on a larger range of concentrations with an earlier generation detector (resolution of ~180eV Mn-Kα), which we present in the Supplementary Material. These results are used to show that even with the older generation detector trace elements can be detected, albeit for higher concentrations, as long as sufficient count time and proper energy settings are used.

2. Material and Methods

2.1 XRF core scanner, sample preparation, and reference standards

All the XCS analyses were acquired using an Avaatech core scanner at the Royal Netherlands Institute for Sea Research (NIOZ). This XRF scanner is equipped with a 100W rhodium (Rh) X-Ray tube and with a Rayspec cubed SiriusSD silicon drift detector with a 40 mm^2 active area of which 30 mm^2 collimated. The detector contains a low capacity preamplifier integrated on the

detector crystal, which allows an improved spectral resolution at short peaking times compared to older generation detectors. The tube energy settings (1-50kV at a maximum of 2 mA), primary beam filters (Aluminium (Al), Palladium (Pd) 'thin' (25 μm), Pd 'thick' (125 μm), and Cu), and measurement times were varied to obtain the optimal settings for trace element analyses. The electric current of the X-Ray source (0-2 mA) was selected to maintain a detector throughput with ~20-40 % dead time (i.e., the time the detector is irresponsive while processing an X-Ray pulse) to minimize sum peak development with relatively high count rates. All the spectral data were processed using bAxil spectrum analysis software, which is developed by Brightspec.

The XRF analyses were performed on wet ("wet-XCS") and dry ("dry-XCS") sediment samples, with a 10x10 mm slit size. The wet sample measurements were acquired directly on the split core surfaces after covering the surface with a 4-μm SPEXCerti Ultralene foil, which prevents dehydration of the sediment and avoids contamination of the measurement prism. Dry sample measurements were performed on freeze dried, thoroughly ground, sediment samples. Polyethylene containers with a circular opening of 15 mm width and 1.5 mm depth were filled with approximately 257±28 mg (1σ; N=79) of material and covered with 4-μm SPEXCerti Ultralene foil.

For consistency control we measured eight external reference standards (GSR-4, GSR-6, GSD-10, JSd-1, JSd-3, MESS 3, SARM 2, and SARM 3), hand pressed in polyethylene containers, before and after every run of XCS measurements (i.e., a core section or a set of 58 polyethylene containers). For these standards we specifically monitored the light elements Al, Ca, and V, as

these are potentially most affected by aging of the detector or variability in helium in the measurement triangle. We tested if the slope (sensitivity) and R^2 (accuracy) values of the regressions (X-Y cross-plots of concentration versus XCS intensities) for Al, Ca, and V were reproducible. Throughout all analyses the slope of the X-Y plot of the reference concentrations to XCS intensities of light elements Al, Ca, and V, varied less than 5%, while the R^2 varied less than 3% for these elements. Repeated analysis throughout the measurement series (N=13) showed a precision (relative standard deviation) of <2% for Al and Ca, and <7% for V. This implies that the analytical setup and performance of the detector remained stable during the entire duration of the experiment. The determination of precision and accuracy for the XCS measurements are discussed in more detail in Section 2.4.

2.2 Mediterranean sediment material to test optimal trace metal method

Samples from an eastern Mediterranean Sea core (MS21PC; 32°20.7'N, 31°39.0'E; 1022 m water depth) (Hennekam et al., 2015; Rohling et al., 2017; Zwiep et al., in press) were used to determine and test the optimal settings for trace metal analyses. Total core length is 751.5 cm, but this study focuses only on the top 1.5 meters and bottom 2 meters of the core, containing sapropel layers S1 (35-95 cm) and S3 (605-660 cm), respectively. These sapropels correspond to well-known intervals of eastern Mediterranean Sea deep-water anoxia (e.g., Rohling et al. 2015). The reference half of the core sections was used for "wet" XCS analyses, while the working half was discretely sampled in 0.5-cm intervals. The discrete samples were measured by ICP-optical emission spectroscopy (ICP-OES) and partially by ICP-MS (approximately every 2-cm intervals, focused around both

145 sapropels) (Hennekam et al., 2015; Zwiep et al., in press). The same discrete samples from the
146 working half of the core were also used for "dry" XCS measurements.
147
148 Before the ICP-OES and ICP-MS measurements, the samples (~125 mg) were totally digested
149 using a procedure with HF-$HClO_4$-HNO_3 acid mixtures (details in Hennekam et al., 2015). The
150 ICP-OES measurements were performed with a Spectro Ciros Vision ICP-OES at Utrecht
151 University. Reference samples (ISE921) indicated a precision and accuracy (relative standard
152 deviation; deviation from reference value) for the ICP-OES measurements: V (3%;±1%), Cr
153 (4%;±4%), Ni(3%;±4%), Cu(3%;±8%), Zn (4%;±2%), and Mo (13%;not available). The ICP-MS
154 measurements were performed with a Thermo Scientific X-Series 2 ICP-MS at Utrecht University.
155 Reference samples (ISE921) indicated a precision and accuracy (relative standard deviation;
156 deviation from reference value) for the ICP-MS measurements: Mo (3%;not available) and U
157 (2%;±7%). No reference value is available for Mo in the ISE921 standard, but Mo measurements
158 performed with both ICP-OES and ICP-OES methods showed an average deviation <13% between
159 the methods.
160
161 *2.3 Testing XCS settings for trace metal analysis*
162 To determine the optimal settings for trace metal analysis by XCS we first focused on 14 samples
163 from the eastern Mediterranean Sea core MS21PC (34, 39, 50, 67, 84, 89, 120, 610, 614, 630, 655,
164 656, 659, and 680 cm depth in the core), which covered a range in concentrations for our target
165 elements (ranges are shown at the top in Table 1). Ground, homogenized, dry sediment samples
166 were used to avoid the impact of physical properties, such as water content, grain size, surface

roughness, and surface slope, potentially biasing XCS results (Tjallingii et al., 2007; Hennekam et al., 2012; Jarvis et al., 2015). Additionally, 8 reference standards (Section 2.1) were included in order to extend the trace-metal concentration range for these tests (see Table 1). The more variable composition of the reference standards may introduce some additional deviations due to matrix effects that are inherent to XRF. Therefore, we present data including and excluding these reference standards (Table 1; Figure 1).

The 14 samples from the eastern Mediterranean Sea and the 8 reference standards were measured with variable tube energy settings, primary beam filters, and measurement times. At first, the XCS measurements were performed with a constant measurement time (10 s) and changing the energy settings of the Rh tube between 10 to 50 kV in steps of 5kV. The primary beam filters (i.e., Al-, Pd-thin-, Pd-thick-, and Cu-filters) were used on all energy settings to reduce the spectral background. This resulted in a set of 35 different XCS settings that were used to analyze the 22 sediment samples in threefold. Based on the results of this test, we selected the settings that showed the most promising results for trace element analysis (i.e., highest R^2 with the traditional discrete sample analyses, see Section 2.4). Subsequently, we examined precision and accuracy of the XCS measurements for different measurement times applied. This was achieved through varying the dwell time (5, 10, 30, 45, 60, and 120 s) at all the selected energy/filter settings, while analyzing the 22 sediment samples in fivefold.

2.4 XCS data precision, accuracy, and calibration

188 The XCS data is initially presented as intensity rates (counts per second; cps), and after evaluation
189 of the optimal settings, the XCS data were converted to concentrations (ppm) using the multivariate
190 log-ratio calibration (MLC) model (Weltje et al., 2015). The optimal settings were evaluated by
191 the optimal count statistics of the intensity records in terms of precision and accuracy. Precision
192 was determined by calculating relative standard deviations (RSD's) of 2 to 4 replicate
193 measurements, which express the standard deviation as percentage of the mean. Accuracy was
194 determined by calculation of the coefficient of determination (R^2) of cross-plots of reference
195 concentrations versus XCS intensity rates.
196
197 Direct comparison of intensities and concentrations provide fast and convenient information of the
198 optimal count statistics for the XCS records, even when reference values are missing or below
199 detection limits. However, bias in XCS intensity records by down-core changes of physical
200 proprieties, measurement geometry, and non-linear matrix effects are best accommodated by the
201 MLC model (Weltje et al., 2015). The MLC was performed using the AvaaXelerate software
202 (Bloemsma, 2015). The automated calibration sample selection option in the software was used to
203 select a first subset of 32 samples for calibration. Extra samples were added to better cover the
204 variability in our target elements. This resulted in a subset of 45 and 42 samples for, respectively,
205 the wet and dry XCS measurements. For Mo the subset was smaller (23 and 22 samples,
206 respectively) as samples with Mo concentrations below the detection limit of the ICP-OES
207 measurements were excluded. Moreover, U was measured by ICP-MS in a lower resolution only,
208 and hence the calibration subset existed of 23 samples for both wet and dry XCS measurements.
209 These calibration samples were subsequently used with the MLC method in AvaaXelerate to

convert all XCS-derived trace metal intensities into concentrations. The accuracy and precision of the MLC method was then assessed using R^2 values of cross-plots of the XCS concentrations to the reference concentrations, and calculation of the RSD's from replicate XCS analyses, respectively.

2.5 Artificially produced laminated sediments

Synthetic V and Mo laminations in a calcite matrix were used to assess whether XCS properly reflects sub-mm-scale variability for elements with highly contrasting XRF penetration depths. The synthetic laminations were produced by (1) resin-embedding a spiked calcite sample, (2) micro drilling grooves in this resin sample, and (3) filling up the grooves with another spiked calcite mixture and resin-embedding it again (Hennekam et al., 2015). These laminations with alternating V and Mo concentrations of ~40 ppm to ~400 ppm were subsequently measured every 0.1 mm using the previously established "optimal settings" (Section 3.1) and a slit size of 0.2 mm (down core) x 7 mm (cross core). A down-core slit size of 0.2 mm was used, because this was the narrowest slit size where the signal-to-noise ratio of the obtained XRF spectra were adequate.

2.6 Matrix effects on trace metals with contrasting weights (V and Mo)

Polyethylene containers filled with pure calcite, quartz, and clay (montmorillonite) matrices spiked with V_2O_5 and MoS_2 were used to evaluate potential matrix effects on V and Mo intensities. Within these three matrices, ten different V and Mo concentrations were set, covering an approximate 0-2000 ppm range (see Hennekam et al., 2015). These mixtures were also analyzed by ICP-OES, ICP-MS, and XRF on glass beads (Hennekam et al., 2015). The averages of these three

conventional methods were subsequently used as "reference" value for comparison to the XCS measurements. These XCS analyses were performed with the established "optimal settings" (Section 3.1) and a slit size of 10 mm (down core) x 10 mm (cross core).

3. Results and Discussion

3.1 Optimal XCS method assessment for trace metal analysis

To assess the optimal XCS method, we first applied different energy settings (10-50kV; in 5kV steps) and different filters (no filter, Al-, Pd-thin-, Pd-thick-, and Cu-filter) on 14 eastern Mediterranean sediment samples and 8 standard samples that were dry, ground, and homogenized. For the different XCS settings we observed variable R^2 values for the trace metals V, Cr, Ni, Cu, Zn, Mo, and U analyzed in the 14 eastern Mediterranean sediment samples (Table 1). High R^2 values for V and Zn, generally exceeding 0.70, show that these two elements can be measured accurately over a wide range of settings. The elements Cr, Ni, and Cu, show moderate R^2 values, in the range of 0.40-0.50 (Table 1), for the sediments from the Mediterranean Sea. However, when including standard samples covering a larger concentration range (Cr: 10-137 ppm, Ni: 7-104 ppm, Cu: 13-426 ppm) R^2 values exceed 0.80 for Cr, Ni, and Cu for some settings (Table 1). Results for Mo show high R^2 values, exceeding 0.85 for most settings between 30-50kV energies with Pd-thick- and Cu-filters applied (Table 1). For U, on the other hand, R^2 values rarely exceed 0.40 (Table 1). Possibly this lack of a close fit between off-line and XCS data is related to counting of U on the L-emission lines, while the other trace metals are measured at their K-lines. This suggests that increasing the measurement times for U would improve the analytical performance (i.e., the signal-to-noise ratio of U in the XRF spectra). Based on these first tests, 19 settings were selected

to evaluate precision and optimal counting times for the XCS measurements (blue highlighted settings in the left column of Table 1). These settings were mainly focused on (1) 10-30kV without filter and with Al and Pd-thin filters for V, Cr, Ni, Cu, and Zn, and (2) 30-50kV with Pd-thick and Cu filters for Mo and U.

The five best settings for each element, based on highest R^2 values, are highlighted in Figure 1. For all of the five settings, precision and accuracy to determine V is high (RSD <10%; $R^2 \geq 0.85$; Figure 1a). For Cr, R^2 values based on the eastern Mediterranean samples alone are lower ($R^2 \geq 0.50$; Figure 1), which likely reflects the narrow concentration range of these samples (97-127 ppm). The R^2 values are much higher for Cr when the standards are included (10-137 ppm; $R^2 \geq 0.90$). The precision for Cr, as indicated by the RSD's, are between 2-15% for most settings. Results for Ni, Cu, and Zn show that a high precision (<5%) is achievable for all these elements, as well as a high accuracy, especially as a wider concentration range is measured (Figure 1c, d, e). Results for Mo showed some high RSD's, which likely reflect the samples below the detection limit (e.g., 5 ppm; Figure 2). However, typically, precision for Mo is better than 20% for concentrations ≥10 ppm (Figure 1f; samples below <10 ppm were excluded here), and high accuracy is achievable ($R^2 \geq 0.90$; Figure 1f). The precision for U is generally better than 30%, while the R^2 values clearly increase with analytical dwell time for U, being higher than 0.5 if dwell times exceed 30 seconds (Figure 1g). The R^2 values for U reach a maximum of approximately 0.80 for the Mediterranean samples and approximately 0.65 when the standards are included (Figure 1g). The lower R^2 values for the samples including the standards, relative to those without the standards, may result from the variable composition of the standards causing additional deviations related to matrix effects on U.

The highest accuracy/precision for trace metals V, Cr, Ni, Cu, Zn, Mo, and U are achieved using: (1) V and Ni at energies between 15-30kV with an Al filter, (2) Cr at energies between 20-30kV with an Al filter, (3) Cu, Zn, and U at energies between 30-45kV with a Pd-thick filter, and (4) Mo at energies between 30-50kV with a Cu filter. The RSD's and R^2 values show that an appropriate measurement time for trace metals V, Cr, Ni, Cu, Zn, Mo is ≥30s, while the measurement time for U should be as high as possible (here a maximum 120s was used). Clearly, all these trace elements benefit from background reduction using a primary beam filter, which is placed between the X-ray tube and the sample. Background reduction using these filters has been common practice for trace-element analysis in conventional XRF analyses (Gedcke et al., 1977; Potts et al., 1984). For XCS the signal-to-noise (peak height to background) also increases when these filters are applied (see Figure 3 for examples of spectra from 20, 30, and 50kV), which significantly improves trace metal analyses.

Several settings show high precision and accuracy for the target elements, but for practical considerations (i.e., highest time efficiency), three settings are selected here for further evaluation (Table 2). The setting at 20kV with an Al filter allows precise/accurate analyses of V, Cr, and Ni. Moreover, high precision/accuracy is obtained for Cu, Zn, and U at 30kV with a Pd-thick filter. Lastly, precise/accurate analysis of Mo is obtained at 50kV with a Cu filter. The latter setting has an additional advantage that it allows the detection of barium (Ba), which is often analyzed in the context of changes in export productivity (e.g., Van Santvoort et al., 1997). Hence, with these three XCS settings a suite of trace elements is covered which are often considered relevant in the context

298 of paleoceanographic studies. These will therefore be considered “optimal” settings for subsequent
299 analyses on a core from the eastern Mediterranean Sea (Table 2). All these subsequent analyses
300 were performed using a 60 s count time, except for the wet-XCS analysis of U (120 s). These
301 optimal settings are almost identical to those achieved using the previous generation Canberra
302 detector on samples covering a larger concentration range (Supplementary Material), indicating
303 that these settings are probably inherent to the method and not the detector as such.
304
305 *3.2 Eastern Mediterranean Sea sediment record*
306 To test our optimized XCS settings for trace-metal analyses, we measured sediment cores from the
307 eastern Mediterranean Sea with known trace-metal distribution. The intervals shown here contain
308 two periods of sustained anoxic conditions at 35-95 cm (Sapropel S1) and 605-660 cm (Sapropel
309 S3). These events are also characterized by elevated concentrations of trace metals often associated
310 with bottom water anoxia (Nijenhuis et al., 1999; Passier et al., 1999; Warning and Brumsack,
311 2000; Zwiep et al., in press). The sediments consist for ≥90% of clay/silt (<63 μm grains; Figure
312 4a), being excellently suited for XCS analyses (Richter et al., 2006). The top sections of the core
313 contain high amounts of interstitial water, with the wettest part containing 60-65 weight % water,
314 while the lower sections are relatively dry with values between 40-50 weight % of water (Figure
315 4b). The dry-XCS measurements of chlorine (Cl) closely follow the water content, while the Cl
316 intensity rates analyzed on the wet core section show much larger deviations, especially in the top
317 sections. This most likely reflects (random) pooling of water under the foil used during the XCS
318 analyses (Kido et al., 2006; Tjallingii et al., 2007; Hennekam and De Lange, 2012), which may
319 potentially also affect trace-metal analyses by XCS.

Figure 4c-i shows the trace-metal composition measured with dry/wet XCS versus ICP-OES/ICP-MS analyses, including R^2 values comparing the XCS analyses with these reference values. Absorption effects of a water film under the foil may be recognized in the V and Cr intensities. This is shown by a dip in wet-XCS intensities at 60-80 cm (Figure 4c, d) corresponding with a peak in Cl intensities in the wet core (Figure 4b). Moreover, V and Cr show lower R^2 values for the wet-XCS measurements relative to the measurements done on dry sediment. The other trace metals do not show similar dips, which probably reflects their higher atomic number and hence higher fluorescence energies, which are less easily absorbed (e.g., Tjallingii et al., 2007). Nonetheless, in sediment with interstitial water contents between 40-50 % (550-750cm), such effects are no longer apparent for V and Cr, with R^2 values being much more similar for wet and dry measurements (Figure 4c, d).

The trace metal data measured by wet and dry XCS show reasonable to high correlations to the conventional analyses on discrete samples (Figure 4c-i). The dry XCS measurements show, generally, the highest correlation to ICP-OES/ICP-MS data. Apart from water film effects, this is likely due to the dry XCS measurements being performed on exactly the same samples as the conventional measurements. The wet XCS measurements may potentially be slightly offset in the depth domain compared to the discrete samples, thereby adding to the uncertainty. Moreover, the core-based XCS analyses were not performed on homogenized powders, which is another source of potential bias. As such, deviations in XCS results for Cu and Zn relative to ICP-OES values may

largely be due to small-scale inhomogeneity in the wet sediment surface compared to the ground sediment samples (Figure 4f and g).

The down-core U concentration profile captures the large-scale trend, as also revealed by ICP-MS measurements, albeit with appreciable more scatter (Figure 4i). Longer dwell times clearly improve the XCS analyses (Section 3.1), as also suggested by measurements done with analysis times of 900 s (Figure 5a). Similarly, several measurements can be condensed into a single data point by calculating of a 15-point moving average (Figure 5b). This shows that the U profiles closely matches the ICP-MS-based concentration trend. The noise in the XCS-based U record likely primarily reflects the relatively low sedimentary concentrations (maximum: ~13 ppm; average: ~6 ppm). Nonetheless, U is an important indicator for sub-oxic conditions (e.g., Tribovillard et al., 2012), and even though these records contain some scatter, they yield important information on initiation/termination of sub-oxic sedimentary conditions.

The results for the elements investigated here show that measuring sedimentary trace-metal content using XCS is feasible. Larger variability in the trace metals, such as present in black shales (Brumsack, 2006), likely result in much higher R^2 values. This is exemplified by the results for Mo (Figure 4h), showing a strong increase during the sapropels, relative to the background values, which results in R^2 values of $\geq$0.95 for both wet and dry XCS analyses. As such, our results show that time- and cost-efficient trace metal data can now be acquired from many depositional environments using XCS, provided that other parameters that affect XCS analyses (e.g., matrix,

grain size) remain relatively constant. These data become especially useful when converted into quantitative concentrations.

The MLC algorithm provides a state-of-the-art approach for calibration of XCS analyses (Weltje et al., 2015), which we applied to our XCS intensity data (Figure 6). Most trace metal concentrations derived by XCS show strong correlation with the concentrations of conventional methods (Figure 6a-g), except for the elements that already strongly deviated as intensity data (e.g., inhomogeneity impact on wet-XCS Cu data). Overall, the elements V, Cr, Ni, Mo, and U show reasonable to high precision/accuracy (Figure 6a, b, c, f, g), while for Ni and Cu this is achieved predominantly for the dry XCS data (Figure 6d, e). For sedimentary records, especially when somewhat drier (<50 weight % water), the MLC approach thus allows fast establishing quantitative trace-metal data, requiring only a minimum amount (~30-40 samples) of conventional data to be generated for calibration purposes. These quantitative trace-metal data are highly complementary to other major and minor elemental data, which can be used to reconstruct past bottom-water anoxia and organic-matter deposition, such as Br (marine organic carbon), Ba (export productivity), Mn (redox transitions through manganese oxides), Fe (pyrites versus iron-oxides), and S (pyrites and other sulfides) (Van Santvoort et al., 1997; Ziegler et al., 2008; Croudace and Rothwell, 2015).

3.3 High-resolution, sub-mm profiles for trace metals with contrasting atomic weights

The XCS analysis of synthetic laminations shows the capability of XCS to capture sub-mm variability in two trace metals (V and Mo) with highly deviating fluorescence energies and potential effects of different penetration depths (Figure 7). The laminae are well recognizable in the XCS

data for both V and Mo, and generally the XCS profiles closely follow the reference data. However, the transitions between two consecutive layers is smoother in the XCS data, compared to the abrupt transition in the reference data. This is likely related to the irradiated surface area of 0.2x7mm, which is large compared to the sharp transitions, and probably also to the penetration depth and related excited volume ("balloon effect") from which the XRF signal originates (Potts et al., 1997). The higher energy X-rays of Mo, relative to V, originate from deeper depths, causing a smoother transition for Mo in comparison to V. This is especially apparent at 5-10 mm when the laminations are closer together (Figure 7d). In geological samples, approximately 90% of the signal comes from 20-30 μm depth for V, while for Mo this is in the order of 600-800 μm depth (Potts et al., 1997). As such, in fine sequences of laminae this may result in somewhat smoothening of signals of heavier elements, but generally sub-mm signals are measured well through XCS. Here, this is exemplified by the elements V and Mo (selected for their contrasting atomic masses), but these results likely also apply to other (trace) elements, presuming that these were measured with good signal-to-noise ratio in the spectra.

3.4 Matrix effects for V in quartz, clay, and calcite samples

We performed XCS analyses on prepared mixtures of common, pure sediment matrices (quartz, clay, calcite) with increasing concentrations of V and Mo to evaluate potential matrix effects on V and Mo intensities (Figure 8a-b). As sample geometry can be considered equal for all these samples, differences are attributed to differences in matrix. In general, within all matrices, regressions are obtained with high R^2 values of ≥ 0.97. However, it is clear that for V in the calcite matrix, the slope is lower than that observed for quartz or clay (Figure 8a), while for Mo the slopes

406 are much more similar between the different matrices (Figure 8b). The different slopes for V likely
407 reflects differences in absorption, which depends on the concentration of the other elements in the
408 matrix (i.e., matrix effects). Calcium (Ca) in calcite is known as an efficient absorber of V
409 fluorescence radiation, as the K-line energies of the V photons lie just above the absorption edge
410 of Ca (Potts, 1987). Hence, this shows that for sediments with a large variability in Ca, which often
411 occurs in the marine environment, correction for these matrix effects might be necessary to
412 properly analyze sedimentary V by XCS.
413
414 A simple way to reduce matrix effects in XRF is by normalization to incoherent (Compton)
415 radiation (e.g., Nesbitt et al., 1976; Croudace and Gilligan, 1990). Matrix absorption may affect
416 trace-metal fluorescence radiation similarly as incoherent scattering of the Rh X-Ray tube radiation
417 (Croudace and Gilligan, 1990). The results improve for the calcite and clay matrices when
418 comparing reference concentrations to $V/Rh_{incoherent}$ ratios instead of V intensities (Figure 8c).
419 However, the slope of the mixtures in a quartz matrix is deviating when this correction is applied.
420 This might be attributed to the non-linear nature of absorption effects that become more apparent
421 when a wider range of concentrations is regarded (Croudace and Gilligan, 1990; Weltje and
422 Tjallingii, 2008). This means that non-linear matrix effects can strongly change depending on the
423 sediment composition. Correcting of the Ca matrix effects on V using the incoherent scattering
424 may thus be reasonable, but only when concentration differences in V and matrix are limited.
425

426 **4. Conclusions**

Sedimentary trace elements are useful indicators to study, e.g., water-column oxygenation, productivity, sediment provenance, and environmental pollution. We show that, in addition to major and minor elements, XCS can now be used to extract information about sedimentary trace-metal (V, Cr, Ni, Cu, Zn, Mo, and U) contents from core material, much faster than traditional techniques. The XCS data show that general trends and variability in trace metals are well-captured (depending on concentration ranges), even for sub-mm resolutions.

Three optimal settings to analyze sediments for our target trace metals arise from our detailed exploration: 20kV with Al primary beam filter (V, Cr, Ni), 30kV with Pd-thick primary beam filter (Cu, Zn, U), and 50kV with Cu primary beam filter (Mo). For individual trace metals (Cr, Ni, Cu, and Zn) other settings may result in slightly better precision/accuracy, but these three settings cover the whole suite of trace metals while limiting the analytical time. For major element analysis, a 10kV run (no filter) can be added, which would warrant a good coverage of the entire range of elements measurable through XCS. Generally, measurements of ≥30 seconds are required to obtain reliable data for trace metals through XCS. The obtained semi-quantitative measurements can be calibrated using low-resolution geochemical data from conventional methods, by application of a multivariate log-ratio calibration approach, which yields good estimates of trace metal concentrations in both wet and dry sediment samples.

The quantitative measurement of trace elements by XCS opens a wide array of new possibilities to produce long-term (paleo-)records on water-column dynamics (particulate shuttling), seafloor

anoxia, organic carbon burial, sediment provenance, environmental pollution, and many other environmental parameters.

Acknowledgements

We acknowledge the constructive comments by two anonymous reviewers, which were helpful to improve the original manuscript. This research is made possible by financial support to the MEDIFLUX-project (855.01.031) and related MIMES cruise, the PALM-project (820.01.005), and the SCANALOGUE-project (ALWOP.2015.113) by the Netherlands Organization for Scientific Research (NWO). This study was also partially carried out under the program of the Netherlands Earth System Science Centre (NESSC), financially supported by the Dutch Ministry of Education, Culture and Science (OCW). We thank Erik van Vilsteren (ICP-MS), Helen de Waard (ICP-MS), and Ton Zalm (ICP-OES) for analytical assistance at the Utrecht University, and captain, crew, and scientific team of MIMES cruise for core recovery. Sander van den Boorn of Shell Global Solutions Int. kindly provided access to the Jordan core material and XRF-core-scan data, which is used in the Supplementary Material.

References

Algeo, T.J., Lyons, T.W., 2006. Mo-total organic carbon covariation in modern anoxic marine environments: Implications for analysis of paleoredox and paleohydrographic conditions. Paleoceanography 21.

Algeo, T.J., Rowe, H., 2012. Paleoceanographic applications of trace-metal concentration data. Chemical Geology 324–325, 6-18.

Algeo, T.J., Tribovillard, N., 2009. Environmental analysis of paleoceanographic systems based on molybdenum-uranium covariation. Chemical Geology 268, 211-225.

Bloemsma, M.R., 2015. Development of a Modelling Framework for Core Data Integration Using XRF Scanning. Ph.D. thesis. Delft University of Technology, The Netherlands, pp. 229.

Bruland, K.W., 1980. Oceanographic distributions of cadmium, zinc, nickel, and copper in the North Pacific. Earth and Planetary Science Letters 47, 176-198.

Brumsack, H.-J., 2006. The trace metal content of recent organic carbon-rich sediments: Implications for Cretaceous black shale formation. Palaeogeography, Palaeoclimatology, Palaeoecology 232, 344-361.

Croudace, I.W., Gilligan, J.M., 1990. Versatile and accurate trace element determinations in iron-rich and other geological samples using x-ray fluorescence analysis. X-Ray Spectrometry 19, 117-123.

Croudace, I.W., Rothwell, R.G., 2015. Micro-XRF Studies of Sediment Cores: Applications of a non-destructive tool for the environmental sciences. Springer Science+Business Media, Dordrecht.

484 Garver, J.I., Royce, P.R., aSmick, T.A., 1996. Chromium and nickel in shale of the Taconic
485 foreland: a case study for the provenance of fine-grained sediments with an ultramafic
486 source, Journal of Sedimentary Research 66, 100-106.
487 Gedcke, D., Elad, E., Denee, P., 1977. An intercomparison of trace element excitation methods for
488 energy-dispersive fluorescence analyzers. X-Ray Spectrometry 6, 21-29.
489 Gibson, K.A., Peterson, L.C., 2014. A 0.6 million year record of millennial-scale climate variability
490 in the tropics. Geophysical Research Letters 41, 969-975.
491 Hennekam, R., De Lange, G.J., 2012. X-ray fluorescence core scanning of wet marine sediments:
492 methods to improve quality and reproducibility of high-resolution paleoenvironmental
493 records. Limnology & Oceanography: Methods 10, 991-1003.
494 Hennekam, R., Jilbert, T., Mason, P.R.D., de Lange, G.J., Reichart, G.-J., 2015. High-resolution
495 line-scan analysis of resin-embedded sediments using laser ablation-inductively coupled
496 plasma-mass spectrometry (LA-ICP-MS). Chemical Geology 403, 42-51.
497 Jarvis, S., Croudace, I.W., Rothwell, R.G., 2015. Parameter optimisation for the ITRAX core
498 scanner. In: Croudace, I.W., Rothwell, R.G. (Eds.), Micro-XRF Studies of Sediment Cores.
499 Springer Science+Business Media, Dordrecht, pp. 535-562.
500 Kido, Y., Koshikawa, T., Tada, R., 2006. Rapid and quantitative major element analysis method
501 for wet fine-grained sediments using an XRF microscanner. Marine Geology 229, 209-225.
502 Nesbitt, R., Mastins, H., Stolz, G., Bruce, D., 1976. Matrix corrections in trace-element analysis
503 by X-ray fluorescence: An extension of the Compton scattering technique to long
504 wavelengths. Chemical Geology 18, 203-213.

505 Nijenhuis, I.A., Bosch, H.J., Sinninghe Damsté, J.S., Brumsack, H.J., De Lange, G.J., 1999.
506 Organic matter and trace element rich sapropels and black shales: a geochemical
507 comparison. Earth and Planetary Science Letters 169, 277-290.
508 Passier, H.F., Bosch, H.-J., Nijenhuis, I.A., Lourens, L.J., Bottcher, M.E., Leenders, A., Sinninghe
509 Damsté, J.S., de Lange, G.J., Leeuw, J.W., 1999. Sulphidic Mediterranean surface waters
510 during Pliocene sapropel formation. Nature 397, 146-149.
511 Potts, P., Webb, P., Watson, J., 1984. Energy-dispersive x-ray fluorescence analysis of silicate
512 rocks for major and trace elements. X-Ray Spectrometry 13, 2-15.
513 Potts, P.J., 1987. A handbook of silicate rock analysis. Blackie, Glasgow and London.
514 Potts, P.J., Williams-Thorpe, O., Webb, P.C., 1997. The bulk analysis of silicate rocks by portable
515 X-ray fluorescence: effect of sample mineralogy in relation to the size of the excited
516 volume. Geostandards and Geoanalytical Research 21, 29-41.
517 Richter, T.O., van der Gaast, S., Koster, B., Vaars, A., Gieles, R., de Stigter, H.C., de Haas, H.,
518 van Weering, T.C.E., 2006. The Avaatech XRF Core Scanner: technical description and
519 applications to NE Atlantic sediments, In: Rothwell, R.G. (Ed.), New Techniques in
520 Sediment Core Analysis. Special Publications. Geological Society, London, pp. 39-50.
521 Rohling, E., Marino, G., Grant, K., 2015. Mediterranean climate and oceanography, and the
522 periodic development of anoxic events (sapropels). Earth-Science Reviews 143, 62-97.
523 Rohling, E.J., Hibbert, F.D., Williams, F.H., Grant, K.M., Marino, G., Foster, G.L., Hennekam, R.,
524 De Lange, G.J., Roberts, A.P., Yu, J., 2017. Differences between the last two glacial
525 maxima and implications for ice-sheet, $\delta^{18}O$, and sea-level reconstructions. Quaternary
526 Science Reviews 176, 1-28.

527 Ruiz, F., 2001. Trace metals in estuarine sediments from the southwestern Spanish coast. Marine
528 Pollution Bullitin 42, 481-489.
529 Sweere, T., van den Boorn, S., Dickson, A.J., Reichart, G.-J., 2016. Definition of new trace-metal
530 proxies for the controls on organic matter enrichment in marine sediments based on Mn,
531 Co, Mo and Cd concentrations. Chemical Geology 441, 235-245.
532 Tjallingii, R., Röhl, U., Kölling, M., Bickert, T., 2007. Influence of the water content on X-ray
533 fluorescence core-scanning measurements in soft marine sediments. Geochem Geophy
534 Geosy 8, doi:10.1029/2006GC001393 Q002004.
535 Tribovillard, N., Algeo, T.J., Lyons, T., Riboulleau, A., 2006. Trace metals as paleoredox and
536 paleoproductivity proxies: An update. Chemical Geology 232, 12-32.
537 Tribovillard, N., Algeo, T.J., Baudin, F., Riboulleau, A., 2012. Analysis of marine environmental
538 conditions based onmolybdenum–uranium covariation—Applications to Mesozoic
539 paleoceanography. Chemical Geology 324–325, 46-58.
540 Van Santvoort, P.J.M., De Lange, G.J., Langereis, C.G., Dekkers, M.J., Paterne, M., 1997.
541 Geochemical and paleomagnetic evidence for the occurence of "missing" sapropels in
542 eastern Mediterranean sediments. Paleoceanography 12, 773-786.
543 Warning, B., Brumsack, H.J., 2000. Trace metal signatures of eastern Mediterranean sapropels.
544 Palaeogeography, Palaeoclimatology, Palaeoecology 158, 293-309.
545 Weltje, G.J., Tjallingii, R., 2008. Calibration of XRF core scanners for quantitative geochemical
546 logging of sediment cores: theory and application. Earth and Planetary Science Letters 274,
547 423-438.

548 Weltje, G.J., Bloemsma, M., Tjallingii, R., Heslop, D., Röhl, U., Croudace, I.W., 2015. Prediction
549 of geochemical composition from XRF core scanner data: a new multivariate approach
550 including automatic selection of calibration samples and quantification of uncertainties, In:
551 Croudace, I.W., Rothwell, R.G. (Eds.), Micro-XRF Studies of Sediment Cores. Springer
552 Science+Business Media, Dordrecht, pp. 507-534.
553 Wirth, S.B., Gilli, A., Niemann, H., Dahl, T.W., Ravasi, D., Sax, N., Hamann, Y., Peduzzi, R.,
554 Peduzzi, S., Tonolla, M., 2013. Combining sedimentological, trace metal (Mn, Mo) and
555 molecular evidence for reconstructing past water-column redox conditions: The example
556 of meromictic Lake Cadagno (Swiss Alps). Geochimica et cosmochimica acta 120, 220-
557 238.
558 Yang, S.Y., Jung, H.S., Lim, D.I., Li, C.X., 2003. A review on the provenance discrimination of
559 sediments in the Yellow Sea. Earth-Science Reviews 63, 93-120.
560 Ziegler, M., Jilbert, T., De Lange, G.J., Lourens, L.J., Reichart, G.-J., 2008. Bromine counts from
561 XRF scanning as an estimate of the marine organic carbon content of sediment cores.
562 Geochemistry, Geophysics, Geosystems 9, Q05009.

563 Zwiep, K.L., Hennekam, R., Donders, T.H., van Helmond, N.A.G.M., de Lange, G.J., Sangiorgi,
564 F., in press. Marine productivity, water column processes and seafloor anoxia in relation to
565 Nile discharge during sapropels S1 and S3. Quaternary Science Reviews

Tables and Captions

Table 1. Results of the XCS settings test for trace element analysis performed on 14 Mediterranean sapropel samples from core MS21PC and 8 standards samples (the latter are only included in the right part of the table). A stepwise increase in energy (5kV per step) and different filters (no filter, Al-, Pd-thin-, Pd-thick-, and Cu-filter) were used, all measured in triplicate with a measurement time of 10 seconds. Shown are the coefficient of determination (R^2) values for linear regressions of element counts from XCS measurements to element concentrations obtained through conventional methods. The concentration ranges of the elements are indicated in the top row. Color coding highlights R^2 values, i.e., red to green is 0.00 to 1.00 respectively (see color legend). Blue highlighted settings (left column) were used for further analyses to determine precision and most efficient measurement times.

	excluding standards							including standards						
Settings (Energy; Filter; Current)	V (124-275 ppm)	Cr (97-127 ppm)	Ni (63-104 ppm)	Cu (54-77 ppm)	Zn (89-137 ppm)	Mo (0-67 ppm)	U* (2-10 ppm)	V (10-275 ppm)	Cr (10-137 ppm)	Ni (7-104 ppm)	Cu (13-426 ppm)	Zn (10-395 ppm)	Mo (0-67 ppm)	U* (1-14 ppm)
10 kV; No filter; 400 µA	0.78	-0.04	0.07	0.02	-0.49			0.89	0.64	-0.27	0.19	0.00		
10 kV; Al filter; 1200 µA	0.76	0.26	0.18	0.02	-0.10			0.89	0.86	0.01	0.41	0.11		
15 kV; No filter; 125 µA	0.80	0.06	0.39	0.00	-0.54		-0.01	0.90	0.74	0.05	0.58	0.04		0.11
15 kV; Al filter; 600 µA	0.88	0.43	0.51	0.34	-0.33		-0.04	0.91	0.91	0.72	0.97	0.54		0.11
20 kV; No filter; 75 µA	0.84	0.36	0.40	0.09	-0.47	-0.04	0.00	0.90	0.81	0.32	0.77	0.18	-0.01	0.00
20 kV; Al filter; 250 µA	0.85	0.50	0.67	0.11	-0.06	-0.02	-0.05	0.92	0.93	0.79	0.97	0.68	-0.04	-0.01
20 kV; Pd-thin filter; 1200 µA	0.68	0.42	0.55	0.71	0.65	0.07	-0.03	0.87	0.92	0.83	0.98	0.92	0.11	-0.06
25 kV; No filter; 50 µA	0.81	0.48	0.48	0.01	-0.48	0.14	0.00	0.88	0.81	0.32	0.88	0.29	0.11	-0.03
25 kV; Al filter; 140 µA	0.77	0.35	0.57	0.49	0.00	0.15	-0.01	0.89	0.92	0.77	0.98	0.77	0.09	-0.03
25 kV; Pd-thin filter; 250 µA	0.72	0.31	0.55	0.57	0.60	0.67	-0.02	0.89	0.88	0.72	0.98	0.92	0.62	-0.07
30 kV; No filter; 35 µA	0.78	0.16	0.37	0.03	-0.38	0.42	-0.03	0.88	0.84	0.48	0.89	0.43	0.37	-0.08
30 kV; Al filter; 85 µA	0.80	0.36	0.56	0.46	0.12	0.45	0.00	0.90	0.91	0.73	0.98	0.82	0.37	-0.12
30 kV; Pd-thin filter; 200 µA	0.62	0.15	0.47	0.69	0.74	0.76	0.02	0.84	0.85	0.68	0.98	0.93	0.74	0.00
30 kV; Pd-thick filter; 1200 µA	0.51	0.30	0.30	0.43	0.52	0.81	0.25	0.74	0.66	0.40	0.98	0.94	0.81	0.18
30 kV; Cu filter; 1200 µA	0.68	0.37	0.36	0.14	0.00	0.93	0.49	0.86	0.72	0.39	0.76	0.63	0.93	0.46
35 kV; No filter; 30 µA	0.81	0.13	0.44	0.17	-0.38	0.59	0.00	0.90	0.82	0.49	0.91	0.49	0.58	-0.08
35 kV; Al filter; 50 µA	0.75	0.36	0.53	0.37	0.28	0.69	0.09	0.89	0.88	0.71	0.97	0.88	0.66	0.03
35 kV; Pd-thin filter; 100 µA	0.58	0.06	0.39	0.39	0.70	0.70	0.03	0.80	0.77	0.61	0.98	0.93	0.65	0.01
35 kV; Pd-thick filter; 1000 µA	0.66	0.19	0.19	0.48	0.74	0.90	0.33	0.83	0.75	0.46	0.98	0.94	0.88	0.17
35 kV; Cu filter; 800 µA	0.53	0.08	0.18	0.17	0.00	0.95	0.63	0.79	0.68	0.21	0.90	0.79	0.95	0.49
40 kV; No filter; 23 µA	0.69	0.41	0.50	0.22	-0.25	0.68	0.00	0.87	0.87	0.55	0.91	0.59	0.62	-0.08
40 kV; Al filter; 35 µA	0.79	0.28	0.50	0.45	0.25	0.70	-0.01	0.89	0.83	0.66	0.97	0.88	0.70	-0.04
40 kV; Pd-thin filter; 50 µA	0.58	0.08	0.44	0.44	0.71	0.71	0.00	0.84	0.75	0.59	0.98	0.93	0.71	0.00
40 kV; Pd-thick filter; 750 µA	0.62	0.10	0.38	0.51	0.70	0.88	0.40	0.84	0.74	0.38	0.98	0.94	0.87	0.29
40 kV; Cu filter; 400 µA	0.53	0.08	0.29	0.26	0.04	0.96	0.40	0.78	0.68	0.12	0.93	0.83	0.96	0.38
45 kV; No filter; 15 µA	0.78	0.21	0.40	0.20	-0.03	0.72	0.00	0.90	0.82	0.50	0.93	0.76	0.63	-0.03
45 kV; Al filter; 20 µA	0.76	0.29	0.54	0.51	0.60	0.65	0.06	0.89	0.85	0.65	0.97	0.92	0.63	0.01
45 kV; Pd-thin filter; 35 µA	0.45	0.14	0.42	0.42	0.63	0.76	0.02	0.78	0.70	0.59	0.98	0.93	0.75	0.01
45 kV; Pd-thick filter; 500 µA	0.52	0.10	0.32	0.47	0.72	0.92	0.10	0.77	0.72	0.46	0.98	0.94	0.90	0.24
45 kV; Cu filter; 200 µA	0.38	0.28	0.27	0.15	0.12	0.96	0.60	0.64	0.46	0.12	0.93	0.90	0.95	0.52
50 kV; No filter; 10 µA	0.66	0.22	0.42	0.23	0.01	0.68	0.01	0.85	0.78	0.60	0.93	0.83	0.62	0.00
50 kV; Al filter; 15 µA	0.75	0.14	0.48	0.19	0.58	0.62	0.02	0.90	0.81	0.66	0.97	0.93	0.60	0.06
50 kV; Pd-thin filter; 30 µA	0.49	0.40	0.45	0.39	0.69	0.79	0.04	0.75	0.70	0.44	0.98	0.96	0.76	0.07
50 kV; Pd-thick filter; 300 µA	0.50	0.03	0.22	0.19	0.63	0.89	0.32	0.74	0.61	0.32	0.98	0.93	0.86	0.29
50 kV; Cu filter; 100 µA	0.24	0.19	0.10	0.24	0.31	0.94	0.33	0.50	0.25	0.03	0.94	0.94	0.94	0.24

*Measured on L lines

Color legend
R^2
0.00
0.10
0.20
0.30
0.40
0.50
0.60
0.70
0.80
0.90
1.00

577 **Table 2.** Instrumental settings ('optimal') used for specific sets of trace elements.

Tube voltage (kV)	Filter	Trace elements analysed	Currents used for Mediterranean sediments (dry; wet) (µA)*
20	Al	V, Cr, Ni	250; 400
30	Pd-thick	Cu, Zn, U	1200; 1300
50	Cu	Mo	100; 200

*Currents should be adjusted to the matrix that is measured (typically to maintain a dead time of ~30%)

578

579

580

Figures and Captions

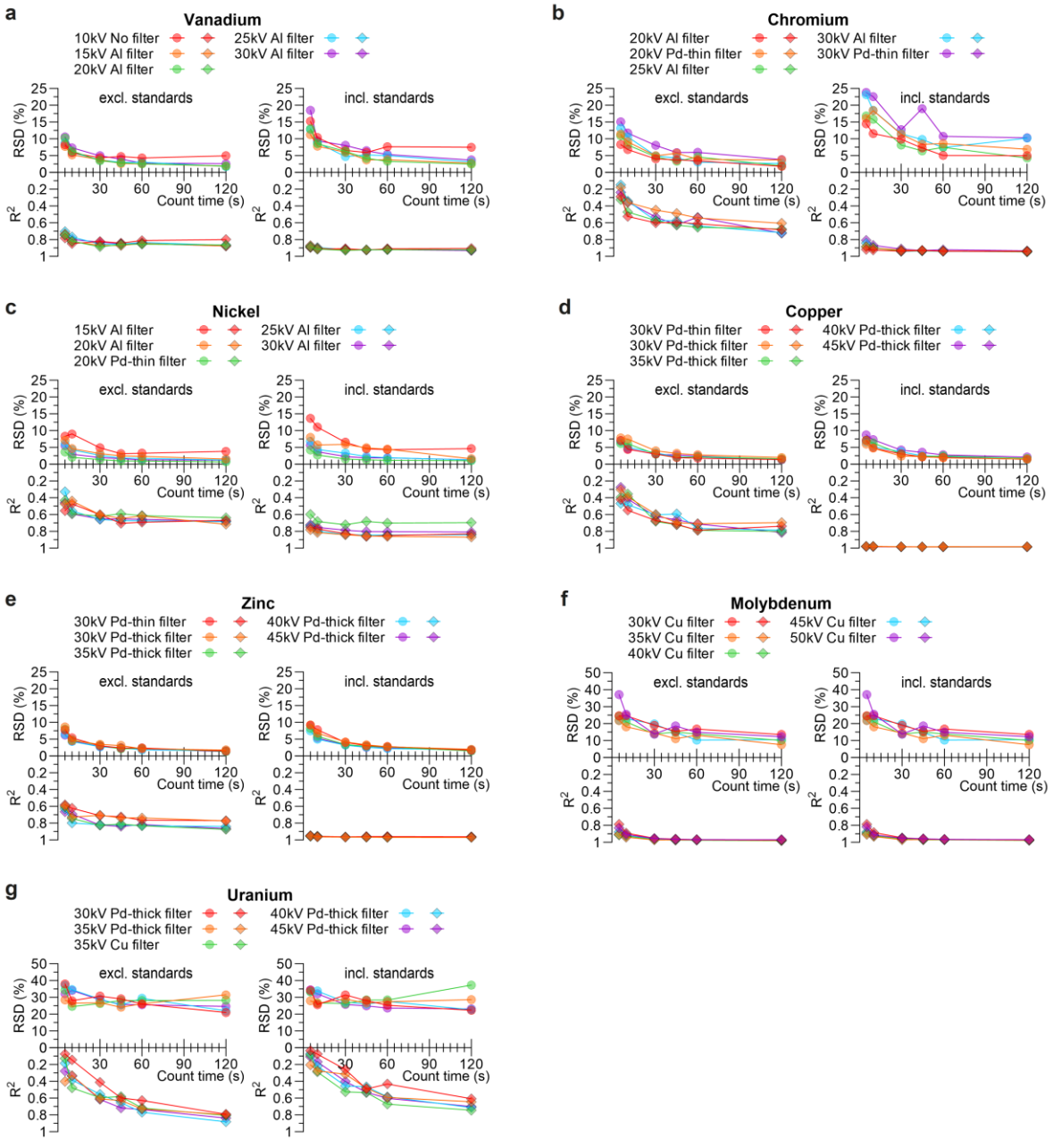

Figure 1. XCS measurement time (5s, 10s, 30s, 45s, 60s, and 120s; X-axis) versus RSD (upper Y-axis) and coefficient of determination (R^2; lower Y-axis). The former are average RSD values combined from all samples, and the latter are

586 determined through regression to concentration values from ICP-OES/ICP-MS measurements. The information for
587 only the five settings that showed the best results (highest R^2) for a trace element are shown (see legends for those
588 specific settings per element). The figure shows the trace elements: (a) V, (b) Cr, (c) Ni, (d) Cu, (e) Zn, (f) Mo, and
589 (g) U. The left panels are for XCS measurements performed on 14 Mediterranean sapropel samples from core MS21PC
590 only, while the right panels also included 8 standard samples. For Mo we only included the samples with Mo
591 concentrations ≥10 ppm to calculate the RSD's, as the samples with lower concentrations were shown to be under the
592 detection limit (see text and Figure 2).

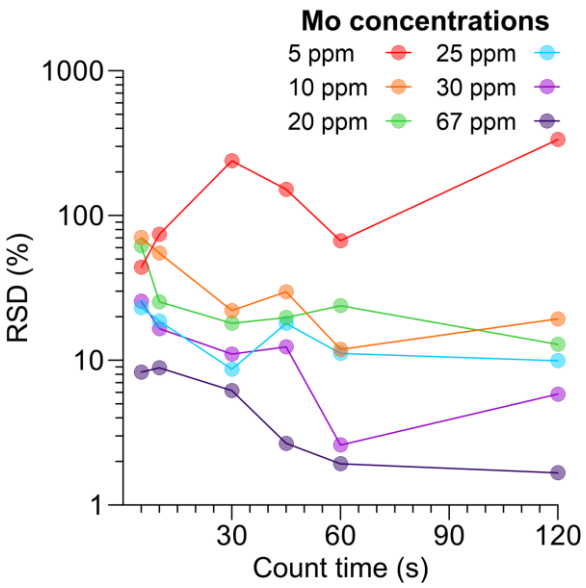

Figure 2. RSD's of Mo (measured at 50kV with a Cu filter) for different sample concentrations. RSD's of XCS measurements of samples with concentrations <10 ppm remain high at all measurement times.

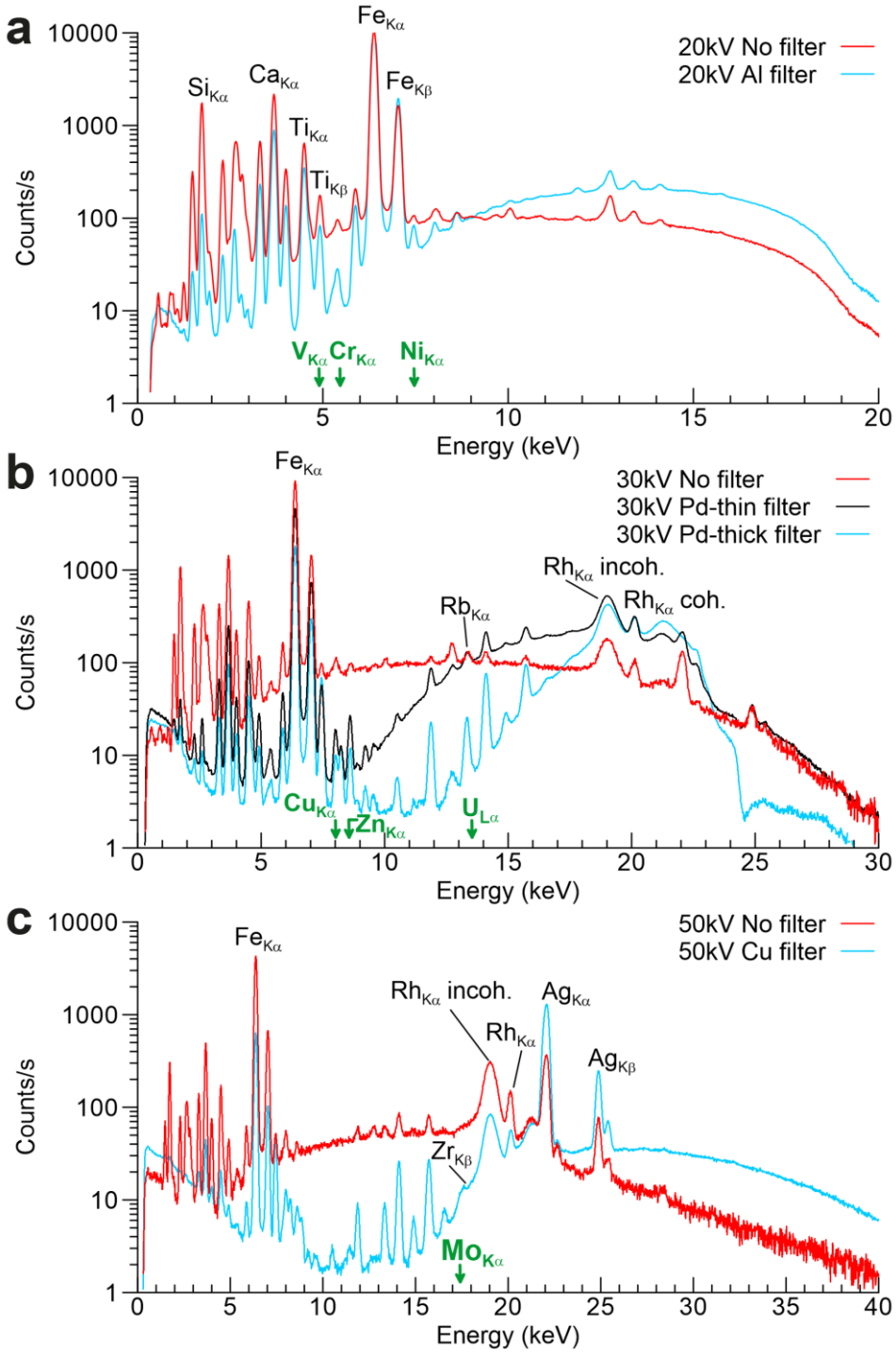

596

597 **Figure 3.** XRF spectra from scans of a Mediterranean sapropel sample (655 cm in core MS21), using settings at 20,

598 30, and 50 kV without and with primary beam filters (Al, Pd-thin, Pd-thick, and Cu filters).

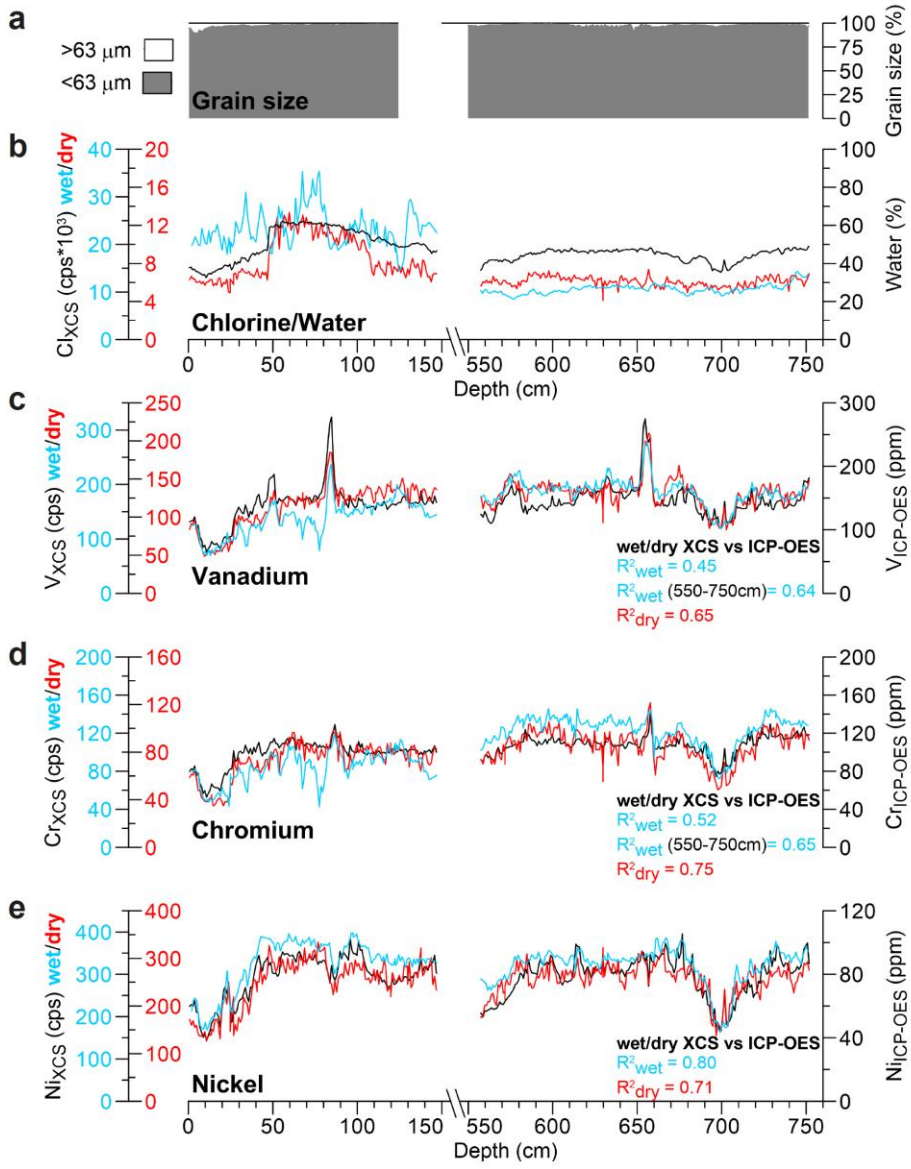

Figure 4. (a) Grain size content (weight % of dry fraction) for core MS21 showing data for particles larger (white) and smaller (grey) than 63μm. (b) The water content of the MS21 sediment, and the Cl intensities measured through XCS for wet and dry MS21 samples. (c-i) Trace metal records for eastern Mediterranean core MS21 on a depth scale. Shown are: V (c), Cr (d), Ni (e), Cu (f), Zn, (g), Mo (h), and U (i). The XCS measurements done on the wet core (blue) and dry sediment samples (red) are shown. Black lines indicate measurements done through ICP-OES, while for Mo and U also ICP-MS measurements are shown with black circles. Correlations between the ICP-OES and/or ICP-MS data with the wet XCS (blue) and dry XCS (red) are shown.

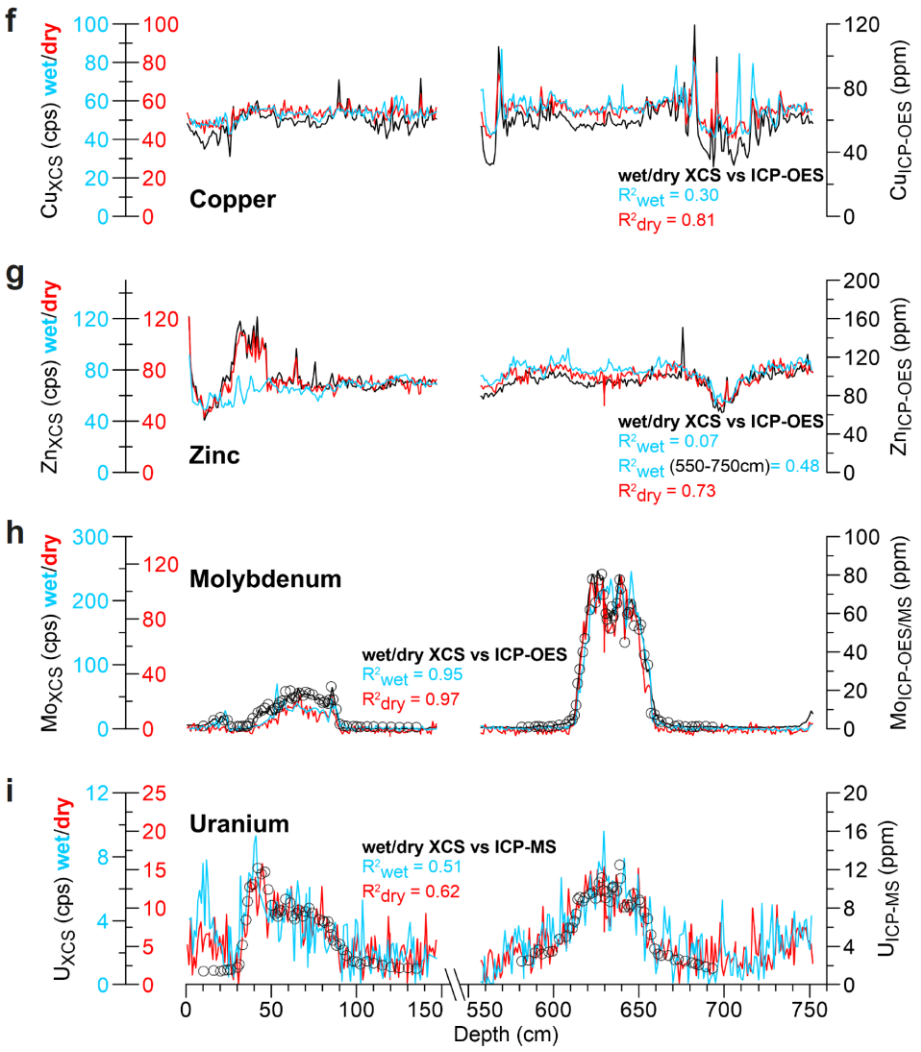

607

608 **Figure 4.** (*continued*).

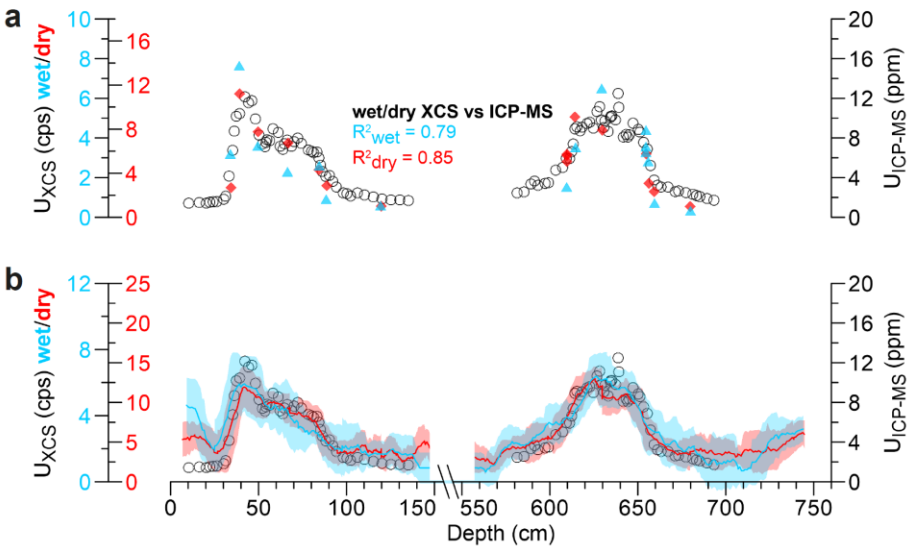

609

610 **Figure 5.** (a) Profile of U in core MS21. The XCS measurement was performed with a 900s measurement time at
611 30kV, with a Pd-Thick filter. The XCS measurements done on the wet core (blue) and dry sediment samples (red) are
612 shown. Black circles indicate measurements done through ICP-MS. (b) Similar to Figure 4i, but with a 15-point moving
613 average for the wet and dry XCS measurements. The shading indicates the 15-point moving standard deviation.

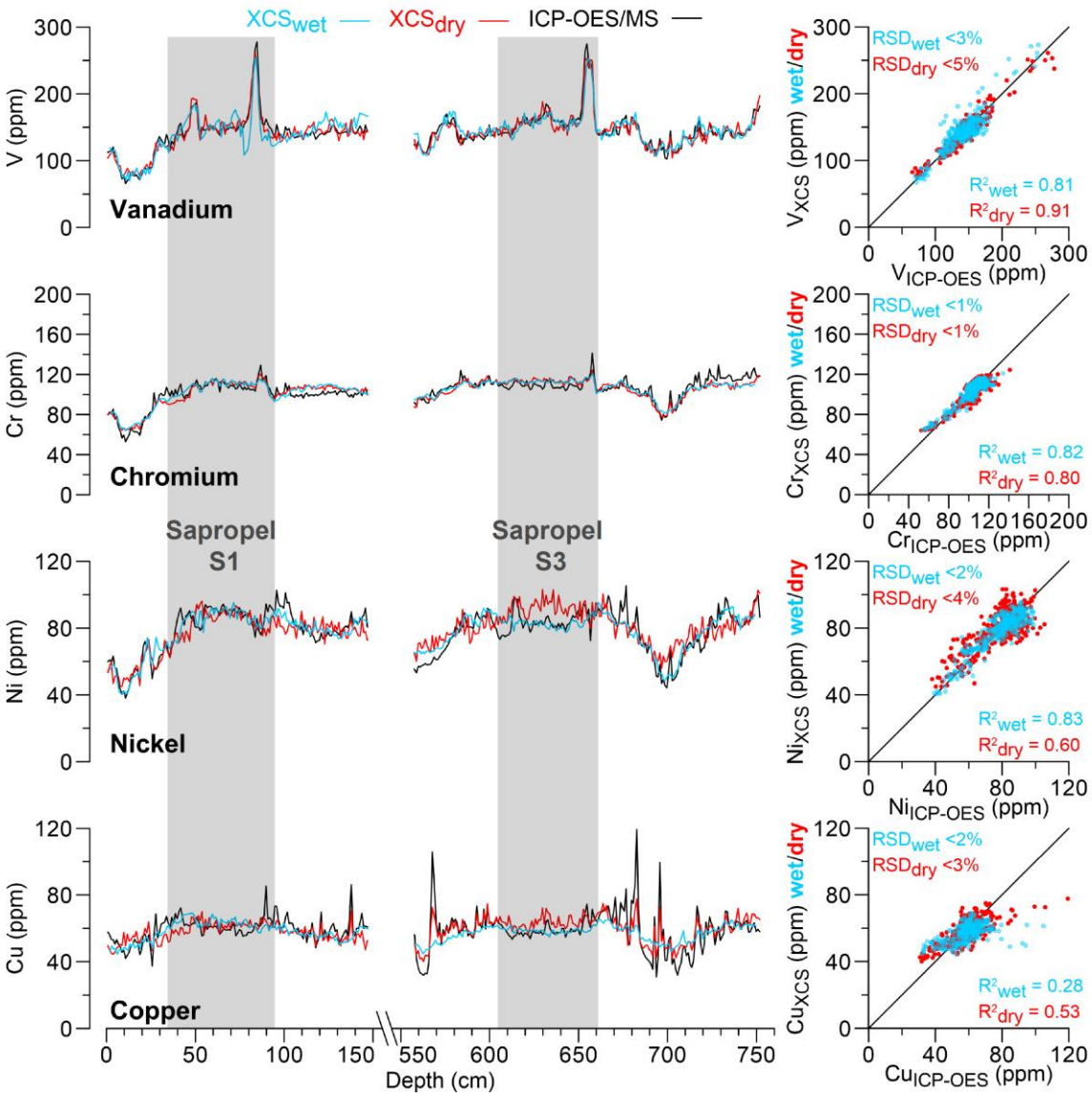

Figure 6. Trace metal concentration records for eastern Mediterranean core MS21 on a depth scale. Shown are: V (a), Cr (b), Ni (c), Cu (d), Zn, (e), Mo (f), and U (g). The XCS intensities, performed on the wet core (blue) and dry sediment samples (red), were converted into concentrations using the MLC approach (Weltje et al., 2015; see Section 2.4). Black lines indicate measurements done through ICP-OES or ICP-MS (for U). The grey areas indicate the positions of Mediterranean sapropels S1 and S3. The right panels show X-Y plots of XCS concentrations (wet XCS in blue and dry XCS in red) versus the ICP-OES/ICP-MS data with their coefficient of determination (R^2). The RSD of replicate measurements are also indicated.

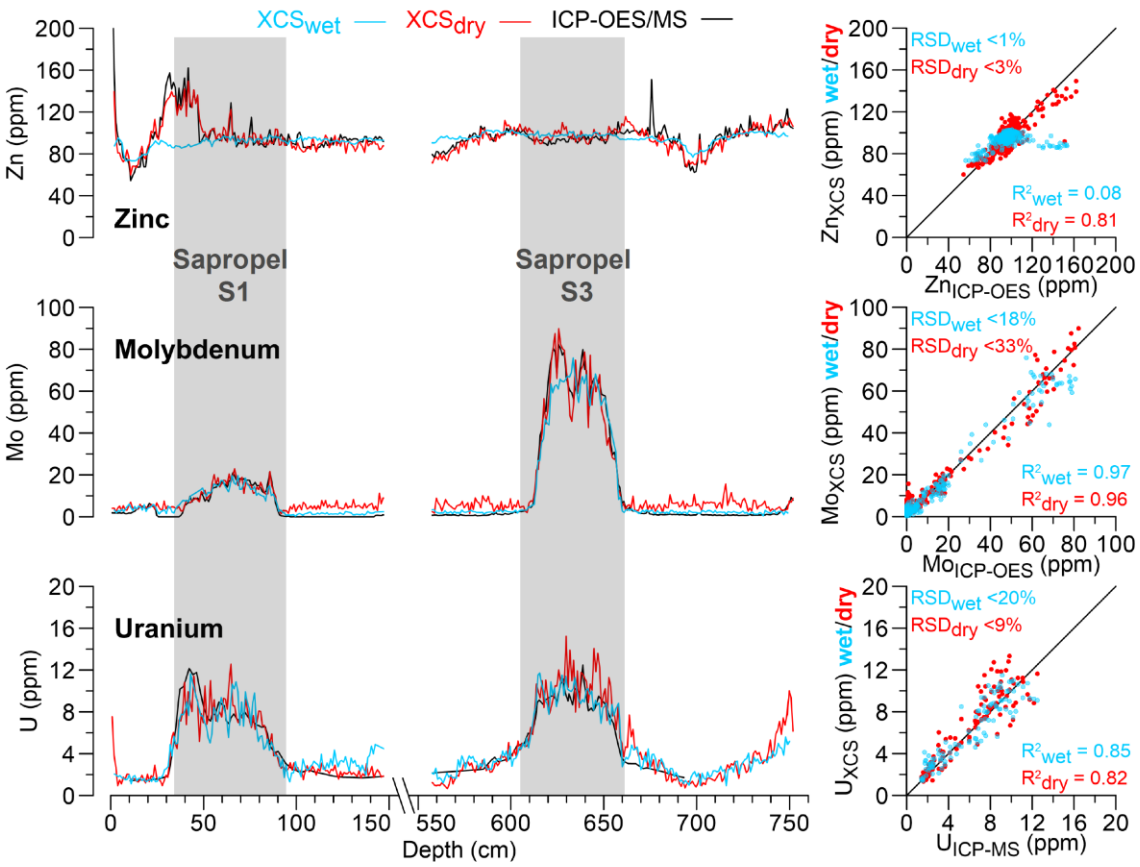

Figure 6. (*continued*).

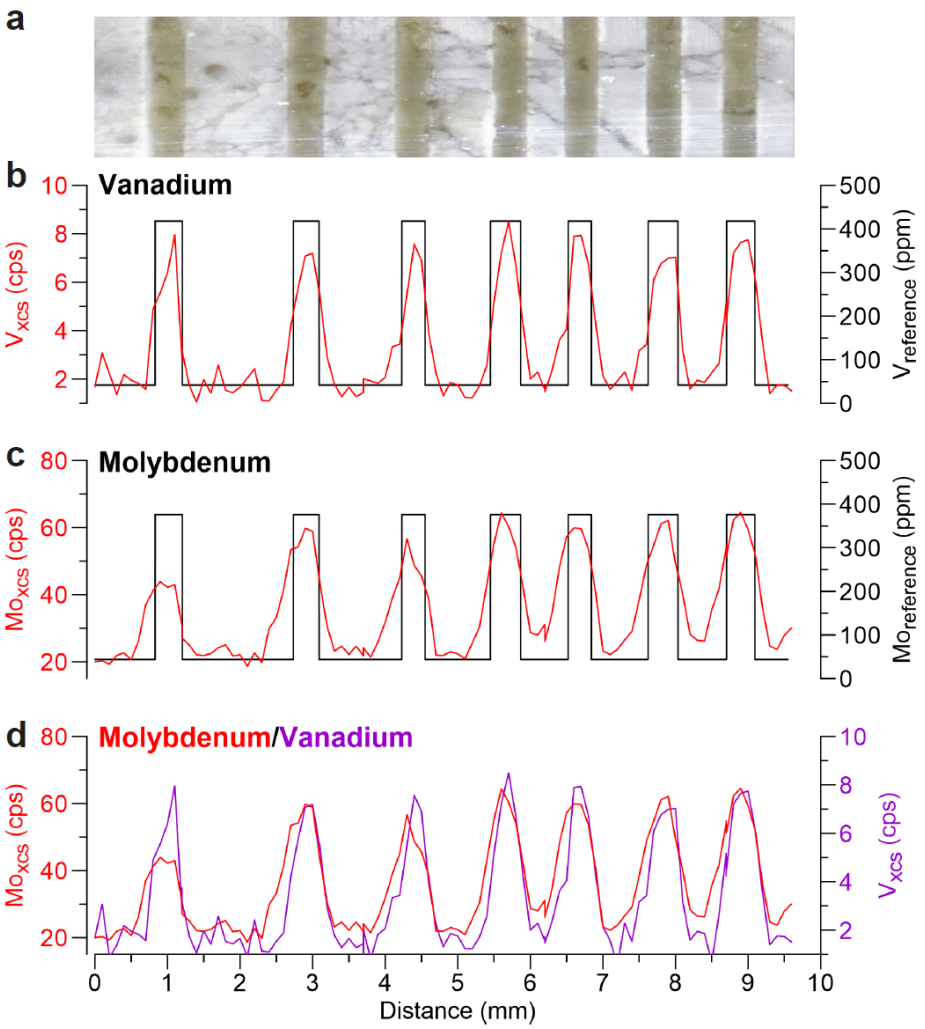

625

626 **Figure 7.** Artificially produced, laminated sediment containing variable concentrations of trace metals with
627 contrasting atomic weights (V and Mo) in a calcite matrix. (a) Picture of the synthetic laminations. (b) XCS
628 measurement of V (red) compared to the reference concentration (black) over a line-scan profile of ~1cm. (c) XCS
629 measurement of Mo (red) compared to the reference concentration (black) over a line-scan profile of ~1cm. (d) Direct
630 comparison of line-scan profiles of Mo (red) and V (purple) measured through XCS.

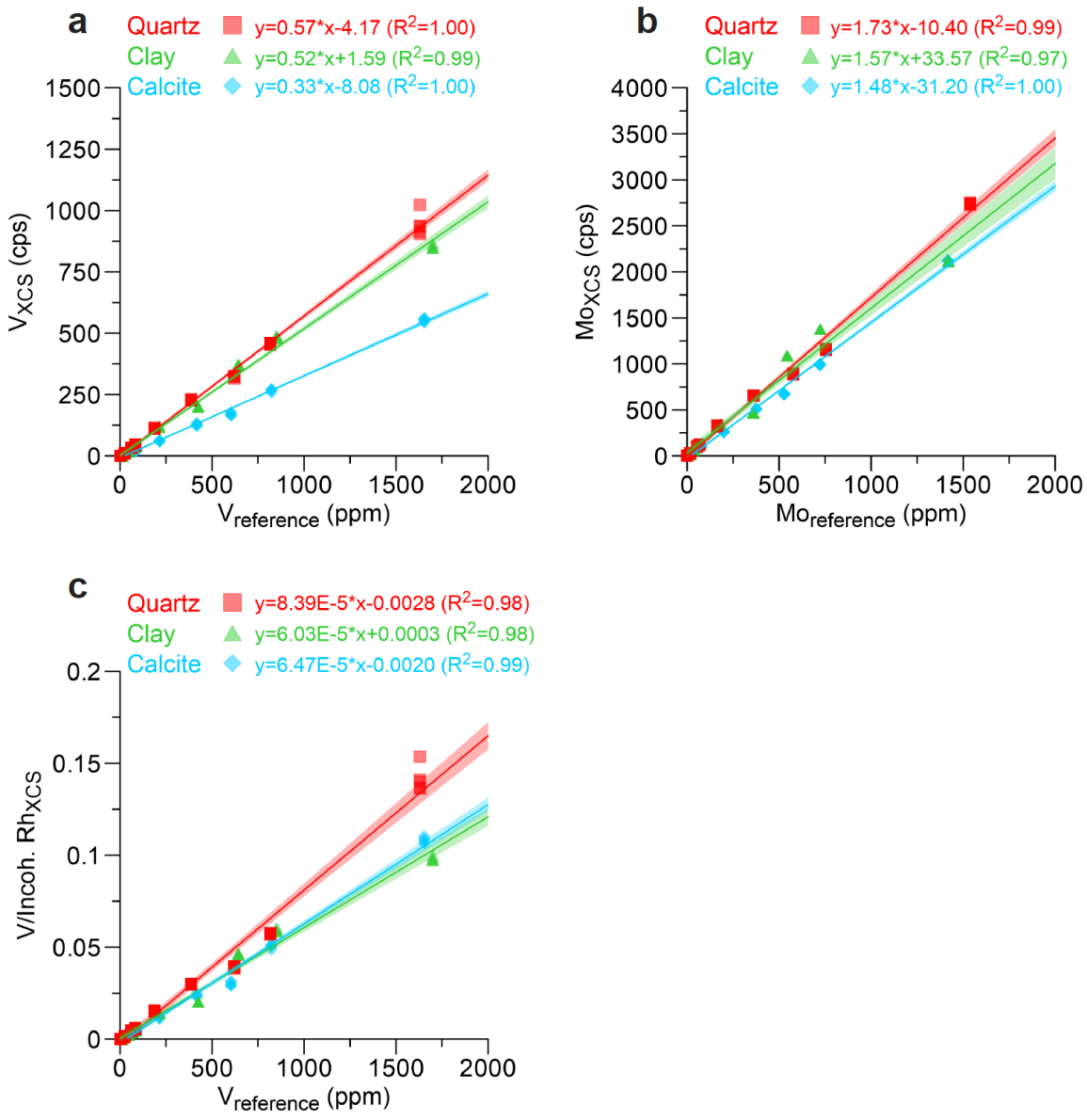

631

632 **Figure 8.** (a) Concentration versus XCS intensity plot for V, with correlations given at the top. (b) Concentration
633 versus XCS intensity plot for Mo. (c) Reference concentrations versus V to Rh incoherent radiation intensity ratios. In
634 all plots the matrices of quartz (red squares), clay (green triangles), and calcite (blue diamonds) are shown. The
635 shadings indicate the 99% confidence intervals of the linear regressions.